DESY–07–161
25th September 2007

Diffractive photoproduction of dijets in *ep* collisions at HERA

ZEUS Collaboration

Abstract

Diffractive photoproduction of dijets was measured with the ZEUS detector at the *ep* collider HERA using an integrated luminosity of $77.2\,\text{pb}^{-1}$. The measurements were made in the kinematic range $Q^2 < 1\,\text{GeV}^2$, $0.20 < y < 0.85$ and $x_{I\!P} < 0.025$, where Q^2 is the photon virtuality, y is the inelasticity and $x_{I\!P}$ is the fraction of the proton momentum taken by the diffractive exchange. The two jets with the highest transverse energy, E_T^{jet}, were required to satisfy $E_T^{\text{jet}} > 7.5$ and $6.5\,\text{GeV}$, respectively, and to lie in the pseudorapidity range $-1.5 < \eta^{\text{jet}} < 1.5$. Differential cross sections were compared to perturbative QCD calculations using available parameterisations of diffractive parton distributions of the proton.

The ZEUS Collaboration

S. Chekanov[1], M. Derrick, S. Magill, B. Musgrave, D. Nicholass[2], J. Repond, R. Yoshida
Argonne National Laboratory, Argonne, Illinois 60439-4815, USA [n]

M.C.K. Mattingly
Andrews University, Berrien Springs, Michigan 49104-0380, USA

M. Jechow, N. Pavel [†], A.G. Yagües Molina
Institut für Physik der Humboldt-Universität zu Berlin, Berlin, Germany [b]

S. Antonelli, P. Antonioli, G. Bari, M. Basile, L. Bellagamba, M. Bindi, D. Boscherini, A. Bruni, G. Bruni, L. Cifarelli, F. Cindolo, A. Contin, M. Corradi, S. De Pasquale[3], G. Iacobucci, A. Margotti, R. Nania, A. Polini, G. Sartorelli, A. Zichichi
University and INFN Bologna, Bologna, Italy [e]

D. Bartsch, I. Brock, H. Hartmann, E. Hilger, H.-P. Jakob, M. Jüngst, O.M. Kind[4], A.E. Nuncio-Quiroz, E. Paul[5], R. Renner[6], U. Samson, V. Schönberg, R. Shehzadi, M. Wlasenko
Physikalisches Institut der Universität Bonn, Bonn, Germany [b]

N.H. Brook, G.P. Heath, J.D. Morris
H.H. Wills Physics Laboratory, University of Bristol, Bristol, United Kingdom [m]

M. Capua, S. Fazio, A. Mastroberardino, M. Schioppa, G. Susinno, E. Tassi
Calabria University, Physics Department and INFN, Cosenza, Italy [e]

J.Y. Kim[7]
Chonnam National University, Kwangju, South Korea

Z.A. Ibrahim, B. Kamaluddin, W.A.T. Wan Abdullah
Jabatan Fizik, Universiti Malaya, 50603 Kuala Lumpur, Malaysia [r]

Y. Ning, Z. Ren, F. Sciulli
Nevis Laboratories, Columbia University, Irvington on Hudson, New York 10027 [o]

J. Chwastowski, A. Eskreys, J. Figiel, A. Galas, M. Gil, K. Olkiewicz, P. Stopa, L. Zawiejski
The Henryk Niewodniczanski Institute of Nuclear Physics, Polish Academy of Sciences, Cracow, Poland [i]

L. Adamczyk, T. Bołd, I. Grabowska-Bołd, D. Kisielewska, J. Łukasik, M. Przybycień, L. Suszycki
Faculty of Physics and Applied Computer Science, AGH-University of Science and Technology, Cracow, Poland [p]

A. Kotański[8], W. Słomiński[9]
Department of Physics, Jagellonian University, Cracow, Poland

V. Adler[10], U. Behrens, C. Blohm, A. Bonato, K. Borras, R. Ciesielski, N. Coppola, V. Drugakov, S. Fang, J. Fourletova[11], A. Geiser, D. Gladkov, P. Göttlicher[12], J. Grebenyuk, I. Gregor, T. Haas, W. Hain, A. Hüttmann, B. Kahle, I.I. Katkov, U. Klein[13], U. Kötz, H. Kowalski, E. Lobodzinska, B. Löhr, R. Mankel, I.-A. Melzer-Pellmann, S. Miglioranzi, A. Montanari, T. Namsoo, D. Notz, L. Rinaldi, P. Roloff, I. Rubinsky, R. Santamarta, U. Schneekloth, A. Spiridonov[14], D. Szuba[15], J. Szuba[16], T. Theedt, G. Wolf, K. Wrona, C. Youngman, W. Zeuner
Deutsches Elektronen-Synchrotron DESY, Hamburg, Germany

W. Lohmann, S. Schlenstedt
Deutsches Elektronen-Synchrotron DESY, Zeuthen, Germany

G. Barbagli, E. Gallo, P. G. Pelfer
University and INFN Florence, Florence, Italy [e]

A. Bamberger, D. Dobur, F. Karstens, N.N. Vlasov[17]
Fakultät für Physik der Universität Freiburg i.Br., Freiburg i.Br., Germany [b]

P.J. Bussey, A.T. Doyle, W. Dunne, M. Forrest, D.H. Saxon, I.O. Skillicorn
Department of Physics and Astronomy, University of Glasgow, Glasgow, United Kingdom [m]

I. Gialas[18], K. Papageorgiu
Department of Engineering in Management and Finance, Univ. of Aegean, Greece

U. Holm, R. Klanner, E. Lohrmann, P. Schleper, T. Schörner-Sadenius, J. Sztuk, H. Stadie, M. Turcato
Hamburg University, Institute of Exp. Physics, Hamburg, Germany [b]

C. Foudas, C. Fry, K.R. Long, A.D. Tapper
Imperial College London, High Energy Nuclear Physics Group, London, United Kingdom [m]

T. Matsumoto, K. Nagano, K. Tokushuku[19], S. Yamada, Y. Yamazaki[20]
Institute of Particle and Nuclear Studies, KEK, Tsukuba, Japan [f]

A.N. Barakbaev, E.G. Boos, N.S. Pokrovskiy, B.O. Zhautykov
Institute of Physics and Technology of Ministry of Education and Science of Kazakhstan, Almaty, Kazakhstan

V. Aushev[1], M. Borodin, A. Kozulia, M. Lisovyi
Institute for Nuclear Research, National Academy of Sciences, Kiev and Kiev National University, Kiev, Ukraine

D. Son
Kyungpook National University, Center for High Energy Physics, Daegu, South Korea [g]

J. de Favereau, K. Piotrzkowski
Institut de Physique Nucléaire, Université Catholique de Louvain, Louvain-la-Neuve, Belgium [q]

F. Barreiro, C. Glasman[21], M. Jimenez, L. Labarga, J. del Peso, E. Ron, M. Soares, J. Terrón, M. Zambrana
Departamento de Física Teórica, Universidad Autónoma de Madrid, Madrid, Spain [l]

F. Corriveau, C. Liu, R. Walsh, C. Zhou
Department of Physics, McGill University, Montréal, Québec, Canada H3A 2T8 [a]

T. Tsurugai
Meiji Gakuin University, Faculty of General Education, Yokohama, Japan [f]

A. Antonov, B.A. Dolgoshein, V. Sosnovtsev, A. Stifutkin, S. Suchkov
Moscow Engineering Physics Institute, Moscow, Russia [j]

R.K. Dementiev, P.F. Ermolov, L.K. Gladilin, L.A. Khein, I.A. Korzhavina, V.A. Kuzmin, B.B. Levchenko[22], O.Yu. Lukina, A.S. Proskuryakov, L.M. Shcheglova, D.S. Zotkin, S.A. Zotkin
Moscow State University, Institute of Nuclear Physics, Moscow, Russia [k]

I. Abt, C. Büttner, A. Caldwell, D. Kollar, W.B. Schmidke, J. Sutiak
Max-Planck-Institut für Physik, München, Germany

G. Grigorescu, A. Keramidas, E. Koffeman, P. Kooijman, A. Pellegrino, H. Tiecke, M. Vázquez[23], L. Wiggers
NIKHEF and University of Amsterdam, Amsterdam, Netherlands [h]

N. Brümmer, B. Bylsma, L.S. Durkin, A. Lee, T.Y. Ling
Physics Department, Ohio State University, Columbus, Ohio 43210 [n]

P.D. Allfrey, M.A. Bell, A.M. Cooper-Sarkar, R.C.E. Devenish, J. Ferrando, B. Foster, K. Korcsak-Gorzo, K. Oliver, S. Patel, V. Roberfroid[24], A. Robertson, P.B. Straub, C. Uribe-Estrada, R. Walczak
Department of Physics, University of Oxford, Oxford United Kingdom [m]

P. Bellan, A. Bertolin, R. Brugnera, R. Carlin, F. Dal Corso, S. Dusini, A. Garfagnini, S. Limentani, A. Longhin, L. Stanco, M. Turcato
Dipartimento di Fisica dell' Università and INFN, Padova, Italy [e]

B.Y. Oh, A. Raval, J. Ukleja[25], J.J. Whitmore[26]
Department of Physics, Pennsylvania State University, University Park, Pennsylvania 16802 [o]

Y. Iga
Polytechnic University, Sagamihara, Japan [f]

G. D'Agostini, G. Marini, A. Nigro
Dipartimento di Fisica, Università 'La Sapienza' and INFN, Rome, Italy [e]

J.E. Cole, J.C. Hart
Rutherford Appleton Laboratory, Chilton, Didcot, Oxon, United Kingdom [m]

H. Abramowicz[27], A. Gabareen, R. Ingbir, S. Kananov, A. Levy, O. Smith, A. Stern
Raymond and Beverly Sackler Faculty of Exact Sciences, School of Physics, Tel-Aviv University, Tel-Aviv, Israel [d]

M. Kuze, J. Maeda
Department of Physics, Tokyo Institute of Technology, Tokyo, Japan [f]

R. Hori, S. Kagawa[28], N. Okazaki, S. Shimizu, T. Tawara
Department of Physics, University of Tokyo, Tokyo, Japan [f]

R. Hamatsu, H. Kaji[29], S. Kitamura[30], O. Ota, Y.D. Ri
Tokyo Metropolitan University, Department of Physics, Tokyo, Japan [f]

M.I. Ferrero, V. Monaco, R. Sacchi, A. Solano
Università di Torino and INFN, Torino, Italy [e]

M. Arneodo, M. Costa, M. Ruspa
Università del Piemonte Orientale, Novara, and INFN, Torino, Italy [e]

S. Fourletov, J.F. Martin, T.P. Stewart
Department of Physics, University of Toronto, Toronto, Ontario, Canada M5S 1A7 [a]

S.K. Boutle[18], J.M. Butterworth, C. Gwenlan[31], T.W. Jones, J.H. Loizides, M. Wing[32]
Physics and Astronomy Department, University College London, London, United Kingdom [m]

B. Brzozowska, J. Ciborowski[33], G. Grzelak, P. Kulinski, P. Łużniak[34], J. Malka[34], R.J. Nowak, J.M. Pawlak, T. Tymieniecka, A. Ukleja, A.F. Żarnecki
Warsaw University, Institute of Experimental Physics, Warsaw, Poland

M. Adamus, P. Plucinski[35]
Institute for Nuclear Studies, Warsaw, Poland

Y. Eisenberg, I. Giller, D. Hochman, U. Karshon, M. Rosin
Department of Particle Physics, Weizmann Institute, Rehovot, Israel [c]

E. Brownson, T. Danielson, A. Everett, D. Kçira, D.D. Reeder[5], P. Ryan, A.A. Savin, W.H. Smith, H. Wolfe
Department of Physics, University of Wisconsin, Madison, Wisconsin 53706, USA [n]

S. Bhadra, C.D. Catterall, Y. Cui, G. Hartner, S. Menary, U. Noor, J. Standage, J. Whyte
Department of Physics, York University, Ontario, Canada M3J 1P3 [a]

[1] supported by DESY, Germany
[2] also affiliated with University College London, UK
[3] now at University of Salerno, Italy
[4] now at Humboldt University, Berlin, Germany
[5] retired
[6] now at Bruker AXS, Karlsruhe, Germany
[7] supported by Chonnam National University in 2006
[8] supported by the research grant no. 1 P03B 04529 (2005-2008)
[9] This work was supported in part by the Marie Curie Actions Transfer of Knowledge project COCOS (contract MTKD-CT-2004-517186)
[10] now at Univ. Libre de Bruxelles, Belgium
[11] now at University of Bonn, Germany
[12] now at DESY group FEB, Hamburg, Germany
[13] now at University of Liverpool, UK
[14] also at Institut of Theoretical and Experimental Physics, Moscow, Russia
[15] also at INP, Cracow, Poland
[16] on leave of absence from FPACS, AGH-UST, Cracow, Poland
[17] partly supported by Moscow State University, Russia
[18] also affiliated with DESY, Germany
[19] also at University of Tokyo, Japan
[20] now at Kobe University, Japan
[21] Ramón y Cajal Fellow
[22] partly supported by Russian Foundation for Basic Research grant no. 05-02-39028-NSFC-a
[23] now at CERN, Geneva, Switzerland
[24] EU Marie Curie Fellow
[25] partially supported by Warsaw University, Poland
[26] This material was based on work supported by the National Science Foundation, while working at the Foundation.
[27] also at Max Planck Institute, Munich, Germany, Alexander von Humboldt Research Award
[28] now at KEK, Tsukuba, Japan
[29] now at Nagoya University, Japan
[30] Department of Radiological Science, Tokyo Metropolitan University, Japan
[31] PPARC Advanced fellow
[32] partially supported by DESY, Germany
[33] also at Łódź University, Poland
[34] Łódź University, Poland
[35] supported by the Polish Ministry for Education and Science grant no. 1 P03B 14129
[†] deceased

[a] supported by the Natural Sciences and Engineering Research Council of Canada (NSERC)

[b] supported by the German Federal Ministry for Education and Research (BMBF), under contract numbers 05 HZ6PDA, 05 HZ6GUA, 05 HZ6VFA and 05 HZ4KHA

[c] supported in part by the MINERVA Gesellschaft für Forschung GmbH, the Israel Science Foundation (grant no. 293/02-11.2) and the U.S.-Israel Binational Science Foundation

[d] supported by the German-Israeli Foundation and the Israel Science Foundation

[e] supported by the Italian National Institute for Nuclear Physics (INFN)

[f] supported by the Japanese Ministry of Education, Culture, Sports, Science and Technology (MEXT) and its grants for Scientific Research

[g] supported by the Korean Ministry of Education and Korea Science and Engineering Foundation

[h] supported by the Netherlands Foundation for Research on Matter (FOM)

[i] supported by the Polish State Committee for Scientific Research, grant no. 620/E-77/SPB/DESY/P-03/DZ 117/2003-2005 and grant no. 1P03B07427/2004-2006

[j] partially supported by the German Federal Ministry for Education and Research (BMBF)

[k] supported by RF Presidential grant N 8122.2006.2 for the leading scientific schools and by the Russian Ministry of Education and Science through its grant Research on High Energy Physics

[l] supported by the Spanish Ministry of Education and Science through funds provided by CICYT

[m] supported by the Particle Physics and Astronomy Research Council, UK

[n] supported by the US Department of Energy

[o] supported by the US National Science Foundation. Any opinion, findings and conclusions or recommendations expressed in this material are those of the authors and do not necessarily reflect the views of the National Science Foundation.

[p] supported by the Polish Ministry of Science and Higher Education as a scientific project (2006-2008)

[q] supported by FNRS and its associated funds (IISN and FRIA) and by an Inter-University Attraction Poles Programme subsidised by the Belgian Federal Science Policy Office

[r] supported by the Malaysian Ministry of Science, Technology and Innovation/Akademi Sains Malaysia grant SAGA 66-02-03-0048

1 Introduction

In diffractive electron-proton scattering, the proton loses a small fraction of its energy and either emerges from the scattering intact, $ep \to eXp$, or dissociates into a low-mass state N, $ep \to eXN$. A large rapidity gap (LRG) separates the hadronic system X with invariant mass M_X and the final-state proton p.

In the framework of Regge phenomenology [1], diffractive interactions are ascribed to the exchange of a trajectory with vacuum quantum numbers, the Pomeron trajectory. In quantum chromodynamics (QCD), the diffractive factorisation theorem [2, 3] states that the diffractive cross section in deep inleastic scattering (DIS) can be expressed as the convolution of universal partonic cross sections and a specific type of parton distribution functions (PDF), the diffractive PDF (dPDF). Diffractive PDFs are interpreted as the number density of partons conditional on the observation of a diffracted proton in the final state. The dPDFs [4–7] have been determined from the HERA inclusive measurements of the diffractive structure function F_2^D [4, 5], defined in analogy with the proton structure function F_2, and were used for input to calculations of hard diffractive processes at HERA, Tevatron and LHC [8–13].

Diffractive collisions producing a state X with a dijet system are a particularly interesting component of diffractive ep interactions. The transverse energies of the jets provide a hard scale, ensuring the applicability of perturbative QCD at the small photon virtualities considered here. In photoproduction, at leading order (LO) of QCD, two types of processes contribute to dijet photoproduction, namely direct and resolved photon processes. In direct photon processes, the exchanged photon participates as a point-like particle, interacting with a gluon from the incoming proton (photon-gluon fusion, Fig. 1a). Thus, these processes are directly sensitive to the gluon content of the diffractive exchange. In resolved photon processes, the photon behaves as a source of partons, one of which interacts with a parton from the diffractive exchange (Fig. 1b). For resolved photon processes, which resemble hadron-hadron interactions, QCD factorisation is not expected to hold [3, 14]. Further interactions between partons from the photon and the proton may fill the rapidity gap, leading to a breakdown of hard-scattering factorisation and causing a suppression of the diffractive photoproduction cross section. Such a mechanism was proposed to explain the suppression of the measured cross sections for hard diffractive hadron-hadron scattering at the Tevatron with respect to expectations based on dPDFs obtained at HERA [15]. For the diffractive resolved photoproduction, an eikonal model [16] predicts a cross-section suppression by about a factor of three. In the framework of another model [17], assuming that diffractive collisions reflect the absorption of an incident particle-wave, it has been argued that the strong factorisation breaking observed in diffractive hadron-induced processes should not be seen in photon-induced processes.

This analysis presents measurements of the diffractive photoproduction of dijets using the ZEUS detector at HERA. A 30-fold increase in luminosity was achieved compared to the previous ZEUS analysis [18]. This, in combination with the addition of a new forward[1] detector, allows measurements to be made in a wider kinematic range. Differential cross sections based on these measurements are compared to next-to-leading-order (NLO) QCD predictions at the hadron level. The comparisons are also made separately for subsamples enriched with direct and resolved photoproduction. A similar study has been recently published by the H1 Collaboration [9].

2 Experimental set-up

This measurement is based on the data taken with the ZEUS detector at the ep collider HERA in 1999-2000 when electrons or positrons of 27.5 GeV were collided with protons of 920 GeV. The sample used for this study corresponds to an integrated luminosity $\mathcal{L} = 77.2\,\mathrm{pb}^{-1}$ ($12.1\,\mathrm{pb}^{-1}$ and $65.1\,\mathrm{pb}^{-1}$ for the e^-p and e^+p samples, respectively)[2]. A detailed description of the ZEUS detector can be found elsewhere [19]. A brief outline of the components that are most relevant for this analysis is given below.

Charged particles are tracked in the central tracking detector (CTD) [20], which operates in a magnetic field of 1.43 T provided by a thin superconducting coil. The CTD consists of 72 cylindrical drift chamber layers, organised in 9 superlayers covering the polar-angle region $15^\circ < \theta < 164^\circ$. The transverse-momentum resolution for full-length tracks is $\sigma(p_T)/p_T = 0.0058 p_T \oplus 0.0065 \oplus 0.0014/p_T$, with p_T in GeV.

The high-resolution uranium-scintillator calorimeter (CAL) [21] consists of three parts: the forward (FCAL), the barrel (BCAL) and the rear (RCAL) calorimeters. Each part is subdivided transversely into towers and longitudinally into one electromagnetic section (EMC) and either one (in RCAL) or two (in BCAL and FCAL) hadronic sections (HAC). The smallest subdivision of the calorimeter is called a cell. The CAL energy resolutions, as measured under test beam conditions, are $\sigma(E)/E = 0.18/\sqrt{E}$ for electrons and $\sigma(E)/E = 0.35/\sqrt{E}$ for hadrons, with E in GeV.

In 1998, the forward plug calorimeter (FPC) [22] was installed in the 20×20 cm^2 beam hole of the FCAL, with a small hole of radius 3.15 cm in the centre to accommodate the beam pipe. The FPC increased the forward calorimetric coverage by about one unit in pseudorapidity to $\eta \lesssim 5$.

---

[1] The ZEUS coordinate system is a right-handed Cartesian system, with the Z axis pointing in the proton beam direction, referred to as the "forward direction", and the X axis pointing left towards the centre of HERA. The coordinate origin is at the nominal interaction point.

[2] From now on, the word "electron" will be used as a generic term for both electron and positron.

The backing calorimeter (BAC) consists of proportional tube chambers placed in the gap of the iron yoke. In the present analysis it was used in conjunction with the CTD and the CAL to identify cosmic muons that traversed the yoke.

The luminosity was measured from the rate of the bremsstrahlung process $ep \to e\gamma p$. The resulting small-angle energetic photons were measured by the luminosity monitor [23], a lead-scintillator calorimeter placed in the HERA tunnel at $Z = -107$ m.

3 Kinematics and reconstruction of variables

Diffractive photoproduction in ep scattering (Fig. 1),

$$e(e) + p(p) \to e(e') + X(X) + p(p'),$$

is described in terms of the four-momenta of the incoming and scattered electrons, e and e', of the incoming and scattered protons, p and p', and of the hadronic system, X. The following kinematic variables are defined: the photon virtuality, $Q^2 = -q^2$, where $q = e - e'$, the squared photon-proton centre-of-mass energy, $W^2 = (p+q)^2$, and the fraction of the electron energy transferred to the proton in its rest frame (inelasticity),

$$y = \frac{p \cdot q}{p \cdot e} \simeq \frac{W^2}{2p \cdot e} \quad .$$

The reaction can be considered to proceed through the interaction of the virtual photon with the diffractive exchange (Pomeron, $I\!P$). This process is described by the invariant mass, M_X, of the hadronic system X and the fraction of the proton momentum carried by the diffractive exchange

$$x_{I\!P} = \frac{(p - p') \cdot q}{p \cdot q} \quad .$$

In the present data, the state X contains a dijet system as the result of a hard scattering process. The partons from the resolved photon and the diffractive exchange participating in the interaction have fractional momenta given by

$$x_\gamma = \frac{p \cdot u}{p \cdot q} \quad ,$$

where u is the four-momentum of the parton in the resolved photon, and

$$z_{I\!P} = \frac{v \cdot q}{(p - p') \cdot q} \quad ,$$

where v is the four-momentum of the parton in the diffractive exchange.

Energy flow objects (EFOs) were reconstructed from CAL clusters and CTD tracks and combine the CTD and CAL information to optimise the resolution of the reconstructed kinematic variables [24]. The EFOs were additionally corrected for energy loss due to inactive material in front of the CAL [25].

The mass M_X of the hadronic system X was reconstructed as

$$M_X = \sqrt{\sum_h (E - p_Z)_h \cdot \sum_h (E + p_Z)_h} \ ,$$

where the index h runs over all EFOs. The quantities E and p_Z indicate the energy and the longitudinal momentum of the EFOs, respectively.

The inelasticity, y, was estimated from the EFOs according to the Jacquet-Blondel method [26] as

$$y_{\mathrm{JB}} = \sum_h (E - p_Z)_h / 2E_e \ ,$$

where E_e is the initial electron energy. For events with an electron candidate, the inelasticity was also determined from the scattered electron, y_e.

The longitudinal momentum fraction transferred from the proton to the diffractive exchange, $x_{I\!P}$, was reconstructed as

$$x_{I\!P} = \sum_h (E + p_Z)_h / 2E_p \ ,$$

where E_p is the initial proton energy.

The jets were reconstructed from the EFOs by using the k_T algorithm [27] in the longitudinally inclusive mode [28] in the laboratory frame. The variables $E_T^{\mathrm{jet1,2}}$ and $\eta^{\mathrm{jet1,2}}$ characterise the two jets with highest transverse energy, E_T, with $E_T^{\mathrm{jet1}} > E_T^{\mathrm{jet2}}$. For the variables x_γ and $z_{I\!P}$, which are not measurable directly, the observable estimators x_γ^{obs} [29] and $z_{I\!P}^{\mathrm{obs}}$ were reconstructed as

$$\begin{aligned} x_\gamma^{\mathrm{obs}} &= \frac{\sum_{\mathrm{jet1,2}} E_T^{\mathrm{jet}} e^{-\eta^{\mathrm{jet}}}}{2yE_e} \ , \\ z_{I\!P}^{\mathrm{obs}} &= \frac{\sum_{\mathrm{jet1,2}} E_T^{\mathrm{jet}} e^{\eta^{\mathrm{jet}}}}{2x_{I\!P}E_p} \ , \end{aligned}$$

where the sums run over the two highest E_T jets.

In direct-photon processes, at LO in QCD, x_γ is equal to one, whereas resolved-photon processes appear at $x_\gamma < 1$. A direct-enriched region was defined by $x_\gamma^{\mathrm{obs}} \geq 0.75$ and a resolved-enriched region by $x_\gamma^{\mathrm{obs}} < 0.75$.

4 Event selection

A three-level trigger system was used to select events online [19, 30]. Events with a large energy deposit in the calorimeter, neglecting the three inner rings of cells around the beampipe in the FCAL, were selected at the first-level trigger. Additional cuts were applied at the second-level trigger to reject beam-gas interactions and other non-*ep* background events. At the third level, the measured transverse energy, excluding the first inner ring of the FCAL, was required to be greater than 11 GeV. Jets were not preselected at any trigger level.

Well-reconstructed events were selected by applying the following quality cuts. The events were required to have at least three well-measured tracks of transverse momentum $p_T >$ 0.2 GeV originating from the same vertex. The longitudinal position of the vertex, $Z_{\rm vtx}$, had to be in the range $-35 < Z_{\rm vtx} < 30\,{\rm cm}$.

Photoproduction events were selected as follows. Events with a scattered electron candidate having an inelasticity of $y_e \leq 0.7$ were assumed to be DIS events and removed. In addition, $0.20 < y_{\rm JB} < 0.85$ was required. The cut on y_e and the upper cut on $y_{\rm JB}$ reduced the remaining background from DIS events and also restricted the range of the virtuality of the exchanged photon to $Q^2 < 1\,{\rm GeV}^2$ with a median value of $10^{-3}\,{\rm GeV}^2$. The lower cut on $y_{\rm JB}$ removed proton-beam gas events which deposit energy in the FCAL near the beam pipe.

Events with at least two jets were selected by requiring a transverse jet energy above $E_T^{\rm jet1(2)} > 7.5\,(6.5)$ GeV. Both jets were required to be in the pseudorapidity range $-1.5 < \eta^{\rm jet1,2} < 1.5$, measured in the laboratory frame.

Diffractive events were selected by requiring the presence of a LRG between the scattered proton and the rest of the hadronic final state. Since the proton was not measured, the requirement of a LRG was implemented by a cut on the total energy in the FPC, $E_{\rm FPC} < 1.0\,{\rm GeV}$, and by demanding $\eta_{\rm max} < 2.8$. Here $\eta_{\rm max}$ is defined as the pseudorapidity of the most forward EFO with an energy above 400 MeV in the CAL. This selection ensures at least a two-unit rapidity gap in the hadronic system, suppressing background from non-diffractive and proton-dissociative processes. In addition, a cut $x_{I\!P} < 0.025$ was applied to enhance the Pomeron-exchange contribution [31].

Finally, cosmic-ray events originating from muons that traversed the detector near the interaction point were removed. Details can be found elsewhere [32, 33]. A total of 6990 events remained after all selection cuts.

5 Monte Carlo simulations

Monte Carlo (MC) simulations were used to determine acceptances and resolution effects at detector level and to extract the hadronisation corrections for the NLO predictions, i.e. ratios of event yields at hadron level to those at parton level.

The MC generator Rapgap [34] was used to simulate dijet processes in diffractive photoproduction at the Born level. Electroweak radiative effects were simulated by using Rapgap in conjunction with Heracles 4.6 [35].

The electron-proton interactions at small Q^2 were modelled with both direct and resolved photon processes (Fig. 1). Events were generated assuming that diffractive processes proceed via the emission of a particle-like Pomeron from the proton followed by the interaction of the virtual photon with the Pomeron. Although this factorised approach has no justification in QCD, it gives a fair description of the data. The diffractive PDFs, as determined by the H1 Collaboration (H1 LO fit 2) [36] for the Pomeron contribution, were used. For resolved photon processes, the photon PDFs GRV-G-HO [37] were chosen.

In the simulation chain, the process of QCD radiation is followed by hadronisation. This was simulated by interfacing Rapgap to a parton-shower model as implemented in Meps [38] and to a hadronisation model based on string fragmentation [39, 40] as implemented in Jetset [41].

The generated MC events were passed through the standard simulation of the ZEUS detector, based on the Geant program [42], and a trigger-simulation package [30]. The simulated events were reconstructed and selected in the same way as the data.

Since the MC events generated with Rapgap did not adequately describe the $z_{IP}^{\rm obs}$ distribution of the data, they were reweighted to the measured distribution separately for $x_\gamma^{\rm obs} \geq 0.75$ and $x_\gamma^{\rm obs} < 0.75$. The relative fractions of direct photon and resolved photon processes were determined from a fit to the data. Resolved processes account for about one third of the total event sample.

Event distributions are compared with the reweighted Rapgap MC distributions for the kinematic variables y, M_X, $E_T^{\rm jet1,2}$ and $\eta^{\rm jet1,2}$ in Fig. 2. The MC distributions were normalised to the data yielding a reasonable overall description of the data.

The hadronisation corrections were calculated with the Rapgap MC sample after reweighting its parton level $z_{IP}^{\rm obs}$ distribution to each of the NLO predictions described in Section 8.2. In addition, hadronisation corrections were also calculated with a MC sample generated with Pomwig [43], a modification of the Herwig MC program [44] based on a cluster fragmentation model [45, 46]. Since only direct photon interactions can be simulated with Pomwig, the comparison to Rapgap was restricted to the range $x_\gamma^{\rm obs} \geq 0.75$.

The bin-by-bin differences between the corrections obtained with the two programs give an indication of the systematic uncertainties due to the hadronisation corrections [33].

The MC generator Pythia [47] was used to model the non-diffractive photoproduction of two jets. Events were generated using the CTEQ5L [48] (GRV-G-HO) parametrisation of the proton (photon) PDFs and processed through the same simulation and selection chain as the data.

6 Background

Background from proton-dissociative events, with a low-mass proton-dissociative system escaping down the beam pipe, was estimated to be $(16 \pm 4)\%$ [32] by fitting to the FPC energy distribution, without the E_{FPC} cut, a mixture of Rapgap and Epsoft MC [49]. This value was also obtained from hard diffractive production of open charm [50]. It was assumed that this estimate is independent of all kinematic variables studied here. The measured cross sections were scaled down accordingly.

Background from non-diffractive dijet photoproduction, as estimated with the Pythia MC, was found to be less than 5% throughout the whole kinematic range, and was neglected.

7 Systematic uncertainties

Systematic uncertainties on the measured cross sections were estimated as described below:

- the trigger efficiency was estimated for both data and Monte Carlo events using an independent trigger branch. The efficiency was above 98% for the entire kinematic range. The Monte Carlo simulation agrees with the data within $\pm 1\%$ [33] and the uncertainty was neglected;
- the transverse jet-energy scale was varied by $\pm 3\%$, the typical uncertainty in this $E_T^{\rm jet}$ range [18]. This variation resulted in an uncertainty of less than $\pm 5\%$;
- the FPC energy cut was varied by $\pm 0.5\,{\rm GeV}$, resulting in an uncertainty less than $\pm 1\%$ in most bins and not more than $\pm 2\%$;
- changing the energy threshold of the EFOs, which is used to calculate $\eta_{\rm max}$, by $\pm 100\,{\rm MeV}$ led to an uncertainty typically less than $\pm 1\%$ and not more than $\pm 2\%$ in any bin;

- the $\eta_{\rm max}$ values of data and Monte Carlo events were shifted relative to each other by ±0.1, the typical η resolution. This led to the largest observed uncertainties which were typically below ±6.5% and up to ±14% for low $z_{I\!P}^{\rm obs}$ and large $x_{I\!P}$ and M_X;
- the lower $y_{\rm JB}$ cut was varied within its resolution (0.04); the resulting uncertainties were typically less than ±1% and not more than ±3%. When the higher $y_{\rm JB}$ cut was lowered, the measured cross sections changed typically by $< 1\%$ and not more than ±4%;
- varying the $\eta^{\rm jet}$ cuts within its resolution (0.1) gave an uncertainty which is mostly below ±1% and not more than ±4%;
- the $x_{I\!P}$ cut was varied within its resolution (0.0025); the resulting uncertainties were typically less than ±2%, increasing to ±6% in the highest M_X and $\eta^{\rm jet1}$ bins.

The systematic uncertainties not associated with the jet-energy scale were added in quadrature to the statistical uncertainty and are shown as error bars of the measured cross sections in Figs 3 to 6. The uncertainty due to the energy scale is shown separately as a shaded band in each of the figures. Overall normalisation uncertainties of ±2.2% from the luminosity determination and of ±4% from subtraction of the dissociative background were not included.

8 Results

8.1 Cross sections

Single-differential cross sections were measured in the kinematic region $Q^2 < 1\,{\rm GeV}^2$, $0.20 < y < 0.85$, $x_{I\!P} < 0.025$, $E_T^{\rm jet1(2)} > 7.5\,(6.5)\,{\rm GeV}$ and $-1.5 < \eta^{\rm jet1,2} < 1.5$, and were determined as a function of y, M_X, $x_{I\!P}$, $z_{I\!P}^{\rm obs}$, $E_T^{\rm jet1}$, $\eta^{\rm jet1}$ and $x_\gamma^{\rm obs}$. The estimated contribution of proton-dissociative background of 16% was subtracted in all bins.

The cross sections are shown in Figs 3 and 4 and listed in Tables 1–3. The cross section dependence on $x_\gamma^{\rm obs}$, shown in Fig. 4, indicates that direct-enriched ($x_\gamma^{\rm obs} \geq 0.75$) processes dominate diffractive dijet photoproduction in the kinematic range of this measurement.

Single-differential cross sections were also determined separately for direct-photon enriched and resolved-photon enriched processes. They are shown in Figs 5 and 6, respectively, and listed in Tables 4 and 5. The two sets of distributions differ in shape. Typically, resolved events are characterised by larger diffractive masses M_X; this in turn reflects into the observed $x_{I\!P}$ behaviour. Slight differences are observed in the $z_{I\!P}^{\rm obs}$ distributions with the most prominent feature being the rise of the direct-enriched component when $z_{I\!P}^{\rm obs}$ approaches one.

8.2 Comparison to the NLO QCD calculations

NLO predictions for diffractive photoproduction of dijets were calculated at parton level with a program by M. Klasen and G. Kramer [51]. The calculations were performed with a fixed-flavour number of $N_f = 4$ and $\Lambda_4 = 330\,\mathrm{MeV}$, chosen to match the value of the running α_S in the region of four active flavours. Three sets of dPDFs were used: the ZEUS LPS fit, determined from an NLO QCD fit to inclusive diffraction and diffractive charm-production data [4], and the H1 2006 fits A and B, obtained from fits to inclusive diffraction data [5]. The Regge-inspired parameters set for the NLO calculations were the same as used to obtain the dPDFs. The t-slope used in the Pomeron flux was $5\,\mathrm{GeV}^2$. For comparison with data, the NLO calculations obtained with the H1 dPDFs were scaled down by a factor[3] of 0.87 [5]. The contribution of subleading Regge trajectories as implemented in the H1 fits was included. For the resolved photon, the γ-PDF parametrisations GRV [37] and AFG04 [52] were used.

The NLO QCD predictions were obtained setting the renormalisation and factorisation scales to $\mu_R = \mu_F = \mu = E_T^{\mathrm{jet1}}$. The theoretical uncertainties were estimated by varying the scales simultaneously between $(0.5 \cdot E_T^{\mathrm{jet1}})$ and $(2 \cdot E_T^{\mathrm{jet1}})$ [51]. Changing the number of active flavours to $N_f = 5$ in the NLO calculations leads to an increase of the expected cross section for $x_\gamma^{\mathrm{obs}} \geq 0.75$ by less than 10%, and to a negligible effect elsewhere. The uncertainties of the dPDFs and the Pomeron flux, constraining directly the normalisation, were not included. The predicted cross sections were transformed to the hadron level using the hadronisation corrections calculated with RAPGAP as described in Section 5. The uncertainties of the hadronisation corrections are not included in the error calculations for the cross sections.

The data are compared with NLO QCD predictions at hadron level for the full x_γ^{obs} range in Figs 3 and 4. The hadronisation corrections applied to the NLO predictions at parton level are shown in the lower part of each plot and the values are given in Tables 1–3. The asymmetric theoretical uncertainties, estimated as described, were determined for the ZEUS LPS fit; those for the other NLO predictions are similar. The data are reasonably well described in shape. However, they lie systematically below all the predictions. Most of the suppression originates from the lower E_T^{jet1} region.

Figure 4(b) shows the ratio of the data and the NLO predictions using the ZEUS LPS fit. The ratio is below one, consistent with a suppression factor of about 0.7 independent of x_γ. Also shown is the ratio expected if the calculated resolved-photon cross section is suppressed by a factor of 0.34 [16]. No additional suppression factor for resolved-enriched

---

[3] The H1 measurements used to derive the H1 dPDFs include low-mass proton-dissociative processes which leads to an overestimate of the photon-diffractive cross section by a factor of $(1.15^{+0.15}_{-0.08})$ as obtained from MC simulations [5].

data is observed. The suppression factor depends on the dPDFs and ranges between about 0.6 (H1 2006 fit A) and about 0.9 (H1 2006 fit B). Within the large uncertainties of NLO calculations, the data are compatible with no suppression, as expected in [17].

Differential cross sections for the direct-enriched and resolved-enriched samples are compared with NLO predictions at hadron level in Figs 5 and 6. Again the hadronisation corrections are shown in the lower part of each plot and the values are given in Tables 4 and 5. For direct-enriched data, the hadronisation corrections are shown for both RAPGAP and POMWIG. The differences are taken as an estimate of the uncertainties as described in Section 5. The data lie systematically below the NLO calculations. Also, contrary to NLO expectations, the cross section as a function of $z_{IP}^{\rm obs}$ for the direct-enriched sample rises steadily with increasing $z_{IP}^{\rm obs}$.

Compared to NLO calculations obtained with the program of Frixione and Ridolfi [53], the H1 Collaboration observed a suppression factor of about 0.5 in both resolved-enriched and direct-enriched cross sections of diffractive dijet photoproduction [9]. The measurements of ZEUS and H1 cover different kinematic regions in E_T and x_{IP}.[4] In particular, the H1 measurements extend to lower E_T values than in the ZEUS analysis. In ZEUS, the largest discrepancy between the measured and predicted values of the cross section is observed at the lowest E_T values suggesting that the conclusion on factorisation breaking depends on the probed scale.

9 Conclusions

Cross sections for diffractive photoproduction of dijets were measured with the ZEUS detector at HERA using an integrated luminosity of $77.2\,{\rm pb}^{-1}$. The measurements were performed in the kinematic region $Q^2 < 1\,{\rm GeV}^2$, $0.20 < y < 0.85$ and $x_{IP} < 0.025$. The two jets with highest transverse energy were required to have $E_T^{\rm jet1(2)} > 7.5\,(6.5)\,{\rm GeV}$ and $-1.5 < \eta^{\rm jet1,2} < 1.5$.

The measured differential cross sections are compared to NLO QCD predictions based on available parameterisations of diffractive PDFs. The comparisons were made for the full data sample as well as for the subsamples enriched with resolved photon ($x_\gamma^{\rm obs} < 0.75$) and direct photon ($x_\gamma^{\rm obs} \geq 0.75$) processes. The NLO calculations tend to overestimate the measured cross sections of both the resolved-enriched and the direct-enriched data sample. However, within the large uncertainties of the NLO calculations the data are compatible with QCD factorisation.

---

[4] It was checked that both programs for calculating NLO predictions give consistent results.

10 Acknowledgements

We are grateful to the DESY directorate for their strong support and encouragment. The effort of the HERA machine group is gratefully acknowledged. We thank the DESY computing and network services for their support. The design, construction and installation of the ZEUS detector has been made possible by the efforts of many people not listed as authors. It is a pleasure to thank M. Klasen and G. Kramer for handing over to us their program for calculating the NLO predictions and for carrying out additional checks.

References

[1] P.D.B. Collins, *An Introduction to Regge Theory and High Energy Physics*, Cambridge University Press (1977);
A.C. Irving and R.P. Worden, Phys. Rept. **34**, 117 (1977);
A.B. Kaidalov, *Regge Poles in QCD,* in M. Shifman (ed.): "At the Frontier of Particle Physics", Vol. 1, p. 603, World Scientific (2002).

[2] L. Trentadue and G. Veneziano, Phys. Lett. **B 323**, 201 (1994);
A. Berera and D.E. Soper, Phys. Rev. **D 53**, 6162 (1996).

[3] J.C. Collins, Phys. Rev. **D 57**, 3051 (1998) ; Erratum ibid. **D 61**, 019902 (2000).

[4] ZEUS Collaboration, S. Chekanov et al., Eur. Phys. J. **C 38**, 43 (2004).

[5] H1 Collaboration, A. Aktas et al., Eur. Phys. J. **C 48**, 749 (2006).

[6] M. Groys, A. Levy and A. Proskuryakov, Proc. of the workshop "HERA and the LHC", H. Jung and A. De Roeck (eds.), CERN-2005-014, DESY-PROC-2005-001, p. 499 (2005), also preprint hep-ph/0601012.

[7] A.D. Martin, M.G. Ryskin and G. Watt, Phys. Lett. **B 644**, 131 (2007).

[8] ZEUS Collaboration, S. Chekanov et al., Eur. Phys. J. **C 51**, 301 (2007).

[9] H1 Collaboration, A. Aktas et al., Eur. Phys. J. **D 51**, 549 (2007).

[10] H1 Collaboration, A.Aktas et al., preprint hep-ex/0610076, also preprint DESY-06-164.

[11] ZEUS Collaboration, S. Chekanov et al., submitted to Eur. Phys. J. **C** (2007), also preprint DESY-07-126.

[12] D. Graudenz and G. Veneziano, Phys. Lett. **B 365**, 302 (1996);
L. Alvero et al., Phys. Rev. **D 59**, 0704022 (1999);
V.A. Khoze, A.D. Martin and M.G. Ryskin, Eur. Phys. J **C 23**, 311 (2002);
C. Royon, Acta Phys. Polon. **B 37**, 3571 (2006).

[13] E. Gotsman et al., preprint hep-ph/0511060, also Proc. of the workshop "HERA and the LHC", H. Jung and A. de Roeck (eds.), CERN-2005-014, DESY-PROC-2005-001, p. 221 (2005).

[14] P.V. Landshoff and J.C. Polkinghorn, Nucl. Phys. **B 33**, 221 (1971) and **B 36**, 642 (1972);
J.C. Collins et al., Phys. Lett. **B 307**, 161 (1993).

[15] CDF Collaboration, T. Affolder et al., Phys. Rev. Lett. **84**, 5043 (2000).

[16] A.B. Kaidalov et al., Eur. Phys. J. **C 21**, 521 (2001);
A.B. Kaidalov et al., Phys. Lett. **B 567**, 61 (2003).

[17] A. Bialas, prepared for 35th Int. Symposium on Multiparticle Dynamics (ISMD 05), Kromeriz, Czech Republic, 9-15 Aug 2005; published in AIP Conf. Proc. **828**, 359 (2006); also in Kromeriz 2005, Multiparticle Dynamics, 359.

[18] ZEUS Collaboration, S. Chekanov et al., Phys. Lett. **B 547**, 164 (2002).

[19] ZEUS Collaboration, U. Holm (ed.), *The ZEUS Detector,* Status Report (unpublished), available on
`http://www-zeus.desy.de/bluebook/bluebook.html`.

[20] N. Harnew et al., Nucl. Inst. Meth. **A 279**, 290 (1989);
B. Foster et al., Nucl. Phys. Proc. Suppl. **B 32**, 181 (1993);
B. Foster et al., Nucl. Inst. Meth. **A 338**, 254 (1994).

[21] M. Derrick et al., Nucl. Inst. Meth. **A 309**, 77 (1991);
A. Andresen et al., Nucl. Inst. Meth. **A 309**, 101 (1991);
A. Caldwell et al., Nucl. Inst. Meth. **A 321**, 356 (1992);
A. Bernstein et al., Nucl. Inst. Meth. **A 336**, 23 (1993).

[22] A. Bamberger et al., Nucl. Inst. Meth. **A 450**, 235 (2000).

[23] J. Andruszków et al., Preprint DESY-92-066, DESY, 1992;
ZEUS Collaboration, M. Derrick et al., Z. Phys. **C 63**, 391 (1994);
J. Andruszków et al., Acta Phys. Pol. **B 32**, 2025 (2001).

[24] G.M. Briskin, Ph.D Thesis, Report DESY-THESIS-1998-036, DESY (1998);
ZEUS Collaboration, J. Breitweg et al., Eur. Phys. J. **C 11**, 35 (1999).

[25] M. Turcato, Ph.D Thesis, Report DESY-THESIS-2003-039, DESY (2003).

[26] F. Jacquet and A. Blondel, *Detection of the Charged Current Event – Method II,* "Proceedings of the Study for an *ep* Facility for Europe", U. Amaldi (ed.), p. 391, Hamburg, Germany (1979), also in preprint DESY 79/48.

[27] S. Catani et al., Nucl. Phys. **B 406**, 187 (1993).

[28] S.D. Ellis and D.E. Soper, Phys. Rev. **D 48**, 3160 (1993).

[29] ZEUS Collaboration, M. Derrick et al., Phys. Lett. **B 348**, 665 (1995).

[30] W.H. Smith et al., Nucl. Inst. Meth. **A 355**, 278 (1995);
W.H. Smith, K. Tokushuku and L.W. Wiggers, "Proc. Computing in High-Energy Physics (CHEP)", Annecy, France, Sept. 1992, C. Verkerk and W. Wojcik (eds.), p. 222, CERN, Geneva, Switzerland (1992), also preprint DESY-92-150B.

[31] K. Golec-Biernat, J. Kwiecinski and A. Szczurek, Phys. Rev. **D 56**, 3995 (1997).

[32] S. Kagawa, Ph.D. Thesis, KEK-report 2005-12 (2006).

[33] R. Renner, Ph.D. Thesis, Bonn-IR-2006-13 (2006).

[34] H. Jung, Comp. Phys. Comm. **86**, 147 (1995).

[35] K. Kwiatkowski, H. Spiesberger and H.J. Möhring, Comp. Phys. Comm. **69**, 155 (1992).

[36] H1 Collaboration, C. Adloff et al., Z. Phys. **C 76**, 613 (1997).

[37] M. Glück, E. Reya and A. Vogt, Phys. Rev. **D 51**, 3220 (1995).

[38] M. Bengtsson and T. Sjöstrand, Z. Phys. **C 37**, 465 (1998).

[39] T. Sjöstrand, Comp. Phys. Comm. **39**, 347 (1986).

[40] T. Sjöstrand and M. Bengtsson, Comp. Phys. Comm. **43**, 367 (1987).

[41] M. Bengtsson and T. Sjöstrand, Comp. Phys. Comm. **46**, 43 (1987); T. Sjöstrand, Comp. Phys. Comm. **82**, 74 (1994).

[42] R. Brun et al., GEANT3, Technical Report CERN-DD/EE/84-1, CERN, 1987.

[43] B.E. Cox and J.R. Forshaw, Comp. Phys. Comm. **144**, 104 (2002).

[44] G. Corcella et al., JHEP **01**, 010 (2001).

[45] B.R. Webber, Preprint hep-ph/9411384, 1994.

[46] M. Schmelling, Physica Scripta **51**, 683 (1995).

[47] T. Sjöstrand, PYTHIA 5.7 *and* JETSET 7.4 *Physics and Manual*, 1993. CERN-TH 7112/93.

[48] CTEQ Collaboration, H.L. Lai et al., Eur. Phys. J. **C 12**, 375 (2000).

[49] M. Kasprzak, Preprint DESY-95-069, 1995.

[50] ZEUS Collaboration, S. Chekanov et al., Nucl. Phys. **B 672**, 3 (2003).

[51] M. Klasen and G. Kramer, Eur. Phys. J. **C 38**, 93 (2004).

[52] P. Aurenche, M. Fontannaz and J. P. Guillet, Eur. Phys. J. **C 44**, 395 (2005).

[53] S. Frixione and S. Ridolfi, Nucl. Phys. **B 507**, 315 (1997).

y bin	$d\sigma/dy$ (pb)	$\delta_{\rm stat}$ (pb)	$\delta_{\rm syst}$ (pb)	$\delta_{\rm ES}$ (pb)	$C_{\rm had}$
0.20, 0.33	137.9	5.3	$^{+15.2}_{-7.0}$	$^{+4.0}_{-2.9}$	1.16
0.33, 0.46	198.4	6.3	$^{+18.9}_{-5.0}$	$^{+12.1}_{-4.1}$	1.09
0.46, 0.59	218.3	6.7	$^{+16.5}_{-10.4}$	$^{+19.4}_{-12.8}$	1.05
0.59, 0.72	196.5	6.2	$^{+19.1}_{-8.2}$	$^{+13.0}_{-5.7}$	1.05
0.72, 0.85	203.6	6.4	$^{+17.1}_{-6.6}$	$^{+16.6}_{-10.4}$	1.04
M_X bin (GeV)	$d\sigma/dM_X$ (pb/GeV)	$\delta_{\rm stat}$ (pb/GeV)	$\delta_{\rm syst}$ (pb/GeV)	$\delta_{\rm ES}$ (pb/GeV)	$C_{\rm had}$
15.0, 20.0	2.11	0.11	$^{+0.11}_{>-0.01}$	$^{+0.13}_{>-0.01}$	1.37
20.0, 25.0	6.35	0.17	$^{+0.24}_{-0.13}$	$^{+0.26}_{-0.23}$	1.16
25.0, 30.0	6.39	0.17	$^{+0.68}_{-0.15}$	$^{+0.51}_{-0.26}$	1.04
30.0, 35.0	5.41	0.17	$^{+0.57}_{-0.32}$	$^{+0.36}_{-0.21}$	1.01
35.0, 40.0	3.14	0.14	$^{+0.62}_{-0.19}$	$^{+0.32}_{-0.13}$	1.01
40.0, 45.0	1.21	0.09	$^{+0.23}_{-0.08}$	$^{+0.21}_{-0.07}$	0.97
$x_{I\!P}$ bin	$d\sigma/dx_{I\!P}$ (nb)	$\delta_{\rm stat}$ (nb)	$\delta_{\rm syst}$ (nb)	$\delta_{\rm ES}$ (nb)	$C_{\rm had}$
0.000, 0.005	0.40	0.06	$^{+0.01}_{-0.04}$	$^{+0.04}_{>-0.01}$	1.46
0.005, 0.010	3.94	0.14	$^{+0.18}_{-0.10}$	$^{+0.14}_{-0.21}$	1.21
0.010, 0.015	6.28	0.17	$^{+0.36}_{-0.10}$	$^{+0.53}_{-0.20}$	1.10
0.015, 0.020	7.00	0.19	$^{+0.84}_{-0.31}$	$^{+0.47}_{-0.27}$	1.02
0.020, 0.025	7.21	0.21	$^{+1.13}_{-0.50}$	$^{+0.62}_{-0.18}$	1.03
$z_{I\!P}^{\rm obs}$ bin	$d\sigma/dz_{I\!P}^{\rm obs}$ (pb)	$\delta_{\rm stat}$ (pb)	$\delta_{\rm syst}$ (pb)	$\delta_{\rm ES}$ (pb)	$C_{\rm had}$
0.2, 0.4	86.4	5.0	$^{+12.4}_{-9.0}$	$^{+9.9}_{-3.6}$	0.88
0.4, 0.6	145.7	4.9	$^{+15.7}_{-8.9}$	$^{+9.3}_{-8.2}$	0.92
0.6, 0.8	192.9	4.9	$^{+9.6}_{-8.0}$	$^{+11.3}_{-10.7}$	1.11
0.8, 1.0	190.2	4.2	$^{+11.2}_{-0.2}$	$^{+10.8}_{-5.2}$	1.49

Table 1: *Differential cross sections for the diffractive photoproduction of dijets as a function of* y*,* M_X*,* $x_{I\!P}$ *and* $z_{I\!P}^{\rm obs}$ *listed with statistical (*$\delta_{\rm stat}$*) and systematic (*$\delta_{\rm syst}$*) uncertainties and energy scale (*$\delta_{\rm ES}$*) uncertainties; the last column shows the hadronisation corrections (*$C_{\rm had}$*) applied to the NLO QCD predictions.*

$E_T^{\rm jet1}$ bin (GeV)	$d\sigma/dE_T^{\rm jet1}$ (pb/GeV)	$\delta_{\rm stat}$ (pb/GeV)	$\delta_{\rm syst}$ (pb/GeV)	$\delta_{\rm ES}$ (pb/GeV)	$C_{\rm had}$
7.5, 9.5	44.0	0.8	$^{+3.9}_{-1.6}$	$^{+0.4}_{-1.0}$	1.02
9.5, 11.5	13.7	0.4	$^{+1.3}_{-0.5}$	$^{+3.1}_{-0.7}$	1.22
11.5, 13.5	3.5	0.2	$^{+0.3}_{-0.2}$	$^{+0.4}_{-0.3}$	1.22
13.5, 15.5	0.8	0.1	$^{+0.1}_{-0.0}$	$^{+0.1}_{-0.1}$	1.35
$\eta^{\rm jet1}$ bin	$d\sigma/d\eta^{\rm jet1}$ (pb)	$\delta_{\rm stat}$ (pb)	$\delta_{\rm syst}$ (pb)	$\delta_{\rm ES}$ (pb)	$C_{\rm had}$
−1.5, −1.0	14.2	0.9	$^{+1.5}_{-0.6}$	$^{+1.0}_{-1.0}$	0.70
−1.0, −0.5	55.6	1.8	$^{+3.1}_{-2.4}$	$^{+3.2}_{-1.9}$	0.94
−0.5, 0.0	72.9	2.0	$^{+5.0}_{-3.6}$	$^{+4.7}_{-3.7}$	1.09
0.0, 0.5	63.6	1.8	$^{+6.3}_{-2.2}$	$^{+4.5}_{-2.6}$	1.16
0.5, 1.0	34.9	1.3	$^{+4.9}_{-0.8}$	$^{+2.3}_{-0.2}$	1.28
1.0, 1.5	8.0	0.6	$^{+1.1}_{-0.3}$	$^{+0.9}_{-0.3}$	1.38

Table 2: *Differential cross sections for the diffractive photoproduction of dijets as a function of* $E_T^{\rm jet1}$ *and* $\eta^{\rm jet1}$ *listed with statistical* ($\delta_{\rm stat}$) *and systematic* ($\delta_{\rm syst}$) *uncertainties and energy scale* ($\delta_{\rm ES}$) *uncertainties ; the last column shows the hadronisation corrections* ($C_{\rm had}$) *applied to the NLO QCD predictions.*

$x_\gamma^{\rm obs}$ bin	$d\sigma/dx_\gamma^{\rm obs}$ (pb)	$\delta_{\rm stat}$ (pb)	$\delta_{\rm syst}$ (pb)	$\delta_{\rm ES}$ (pb)	$C_{\rm had}$
0.250, 0.375	28.5	2.4	$^{+1.4}_{-3.0}$	$^{+0.5}_{-1.1}$	1.23
0.375, 0.500	52.7	3.2	$^{+2.7}_{-4.1}$	$^{+4.2}_{-1.9}$	1.04
0.500, 0.625	78.1	3.7	$^{+3.2}_{-4.2}$	$^{+1.9}_{-4.5}$	1.01
0.625, 0.750	114.3	4.5	$^{+6.8}_{-7.4}$	$^{+5.9}_{-7.3}$	1.18
0.750, 1.000	356.5	6.2	$^{+29.1}_{-14.1}$	$^{+23.3}_{-14.4}$	1.07

Table 3: *Differential cross sections for the diffractive photoproduction of dijets as a function of* $x_\gamma^{\rm obs}$ *listed with statistical* ($\delta_{\rm stat}$) *and systematic* ($\delta_{\rm syst}$) *uncertainties and energy scale* ($\delta_{\rm ES}$) *uncertainties; the last column shows the hadronisation corrections applied to the NLO QCD predictions.*

y bin	$d\sigma/dy$ (pb)	δ_{stat} (pb)	δ_{syst} (pb)	δ_{ES} (pb)	C_{had}
0.20, 0.33	123.2	5.1	$^{+12.0}_{-6.7}$	$^{+2.3}_{-3.8}$	1.10
0.33, 0.46	152.6	5.7	$^{+13.0}_{-4.5}$	$^{+10.2}_{-4.8}$	1.07
0.46, 0.59	151.8	5.7	$^{+11.0}_{-7.3}$	$^{+13.6}_{-8.5}$	1.07
0.59, 0.72	125.2	5.0	$^{+13.4}_{-5.3}$	$^{+7.9}_{-1.8}$	1.05
0.72, 0.85	135.3	5.4	$^{+11.3}_{-4.9}$	$^{+10.6}_{-9.8}$	1.09
M_X bin (GeV)	$d\sigma/dM_X$ (pb/GeV)	δ_{stat} (pb/GeV)	δ_{syst} (pb/GeV)	δ_{ES} (pb/GeV)	C_{had}
15.0, 20.0	2.08	0.11	$^{+0.10}_{-0.01}$	$^{+0.13}_{>-0.01}$	1.37
20.0, 25.0	5.27	0.16	$^{+0.30}_{-0.08}$	$^{+0.22}_{-0.13}$	1.11
25.0, 30.0	4.88	0.16	$^{+0.38}_{-0.17}$	$^{+0.35}_{-0.35}$	1.05
30.0, 35.0	3.26	0.14	$^{+0.36}_{-0.25}$	$^{+0.23}_{-0.14}$	1.03
35.0, 40.0	1.70	0.11	$^{+0.36}_{-0.16}$	$^{+0.19}_{-0.06}$	1.05
40.0, 45.0	0.58	0.07	$^{+0.12}_{-0.07}$	$^{+0.12}_{-0.07}$	1.05
$x_{I\!P}$ bin	$d\sigma/dx_{I\!P}$ (nb)	δ_{stat}	δ_{syst}	δ_{ES}	C_{had}
0.000, 0.005	0.40	0.06	$^{+0.01}_{-0.05}$	$^{+0.03}_{>-0.01}$	1.48
0.005, 0.010	3.33	0.12	$^{+0.18}_{-0.05}$	$^{+0.14}_{-0.15}$	1.22
0.010, 0.015	4.84	0.15	$^{+0.27}_{-0.09}$	$^{+0.34}_{-0.16}$	1.10
0.015, 0.020	4.86	0.16	$^{+0.56}_{-0.26}$	$^{+0.34}_{-0.22}$	1.06
0.020, 0.025	4.43	0.18	$^{+0.68}_{-0.40}$	$^{+0.34}_{-0.21}$	1.03
$z_{I\!P}^{\text{obs}}$ bin	$d\sigma/dz_{I\!P}^{\text{obs}}$ (pb)	δ_{stat} (pb/GeV)	δ_{syst} (pb/GeV)	δ_{ES} (pb/GeV)	C_{had}
0.2, 0.4	72.0	4.7	$^{+9.1}_{-8.1}$	$^{+7.4}_{-3.3}$	0.89
0.4, 0.6	105.3	4.2	$^{+12.3}_{-5.6}$	$^{+6.5}_{-7.1}$	1.02
0.6, 0.8	120.6	3.8	$^{+9.5}_{-3.1}$	$^{+8.0}_{-4.8}$	1.17
0.8, 1.0	144.0	3.8	$^{+4.4}_{-2.4}$	$^{+7.3}_{-5.2}$	1.59

Table 4: *Differential cross sections for the diffractive photoproduction of dijets for* $x_\gamma^{\text{obs}} \geq 0.75$ *listed with statistical* (δ_{stat}) *and systematic* (δ_{syst}) *uncertainties and energy scale* (δ_{ES}) *uncertainties; the last column shows the hadronisation corrections applied to the NLO QCD predictions.*

y bin	$d\sigma/dy$ (pb)	δ_{stat} (pb)	δ_{syst} (pb)	δ_{ES} (pb)	C_{had}
0.20, 0.33	14.7	1.5	$^{+2.5}_{-1.0}$	$^{+0.7}_{-0.1}$	1.93
0.33, 0.46	44.9	2.7	$^{+5.6}_{-2.7}$	$^{+0.1}_{-1.7}$	1.19
0.46, 0.59	66.5	3.5	$^{+11.9}_{-6.9}$	$^{+3.9}_{-5.9}$	1.01
0.59, 0.72	71.0	3.6	$^{+22.4}_{-4.4}$	$^{+3.6}_{-5.0}$	1.08
0.72, 0.85	69.5	3.5	$^{+18.6}_{-4.5}$	$^{+4.3}_{-2.8}$	1.09
M_X bin (GeV)	$d\sigma/dM_X$ (pb/GeV)	δ_{stat} (pb/GeV)	δ_{syst} (pb/GeV)	δ_{ES} (pb/GeV)	C_{had}
15.0, 20.0	0.03	0.01	$^{+0.01}_{-0.01}$	$^{<+0.01}_{>-0.01}$	1.72
20.0, 25.0	1.09	0.07	$^{<+0.01}_{-0.15}$	$^{+0.04}_{-0.11}$	1.54
25.0, 30.0	1.55	0.07	$^{+0.27}_{-0.07}$	$^{+0.06}_{-0.04}$	1.07
30.0, 35.0	2.14	0.10	$^{+0.59}_{-0.18}$	$^{+0.07}_{-0.14}$	1.01
35.0, 40.0	1.45	0.09	$^{+0.50}_{-0.14}$	$^{+0.07}_{-0.12}$	1.11
40.0, 45.0	0.64	0.06	$^{+0.26}_{-0.06}$	$^{+0.07}_{-0.04}$	1.08
x_{IP} bin	$d\sigma/dx_{IP}$ (nb)	δ_{stat} (nb)	δ_{syst} (nb)	δ_{ES} nb)	C_{had}
0.005, 0.010	0.60	0.05	$^{<+0.01}_{-0.07}$	$^{<+0.01}_{-0.07}$	1.16
0.010, 0.015	1.44	0.08	$^{+0.20}_{-0.09}$	$^{+0.13}_{-0.08}$	1.13
0.015, 0.020	2.19	0.10	$^{+0.46}_{-0.13}$	$^{+0.04}_{-0.14}$	1.08
0.020, 0.025	2.76	0.12	$^{+0.99}_{-0.28}$	$^{+0.15}_{-0.11}$	1.13
z_{IP}^{obs} bin	$d\sigma/dz_{IP}^{\text{obs}}$ (pb)	δ_{stat} (pb)	δ_{syst} (pb)	δ_{ES} (pb)	C_{had}
0.2, 0.4	14.4	1.8	$^{+8.5}_{-1.5}$	$^{+1.8}_{-0.9}$	0.96
0.4, 0.6	40.4	2.6	$^{+22.3}_{-3.7}$	$^{+2.5}_{-1.4}$	0.95
0.6, 0.8	72.3	3.1	$^{+20.7}_{-5.6}$	$^{+3.8}_{-5.5}$	1.19
0.8, 1.0	46.2	1.8	$^{+0.8}_{-11.3}$	$^{+0.8}_{-2.7}$	1.26

Table 5: *Differential cross sections for the diffractive photoproduction of dijets for* $x_\gamma^{\text{obs}} < 0.75$ *listed with statistical* (δ_{stat}) *and systematic* (δ_{syst}) *uncertainties and energy scale* (δ_{ES}) *uncertainties; the last column shows the hadronisation corrections applied to the NLO QCD predictions.*

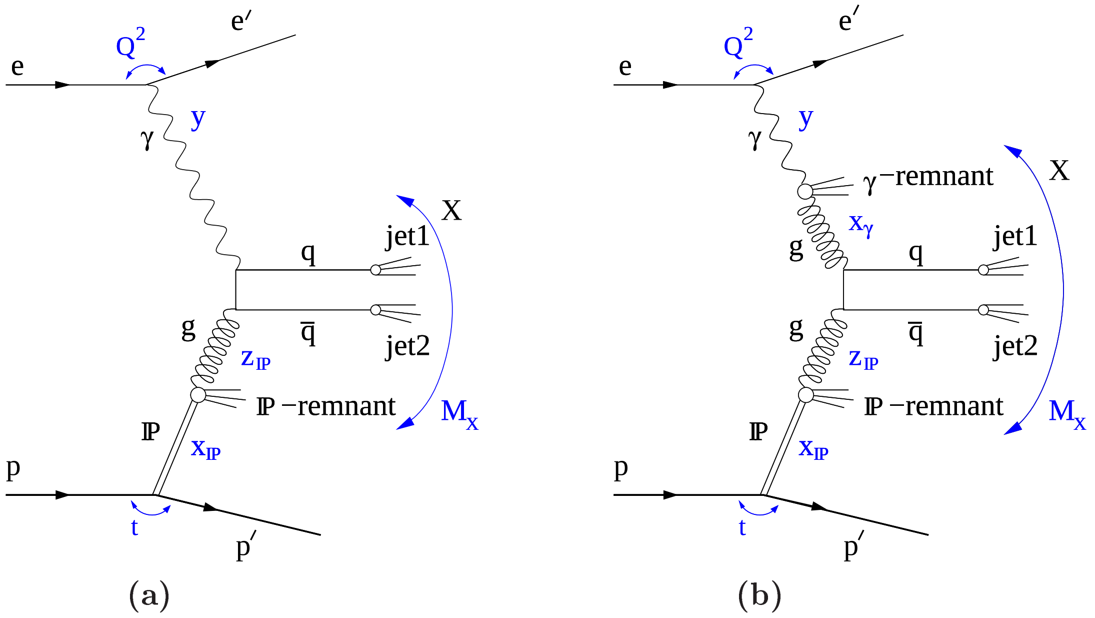

Figure 1: *Leading-order diagrams for (a) direct and (b) resolved processes in diffractive photoproduction of dijets at HERA. The variables shown in the plots are described in the text.*

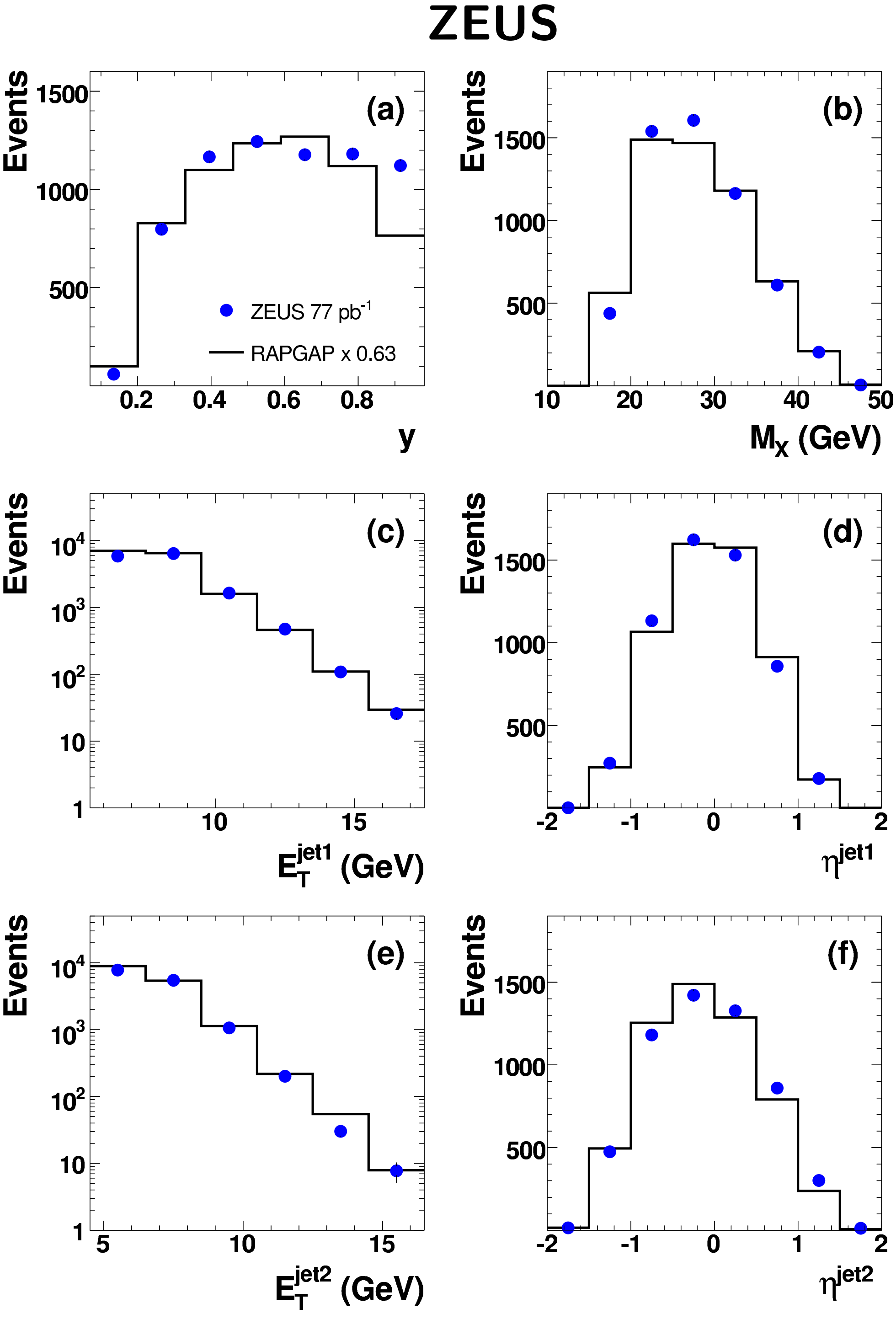

Figure 2: *Comparison of the data (dots) with the* RAPGAP MC *(solid line) normalised to the data as a function of (a) y, (b) M_X, (c) E_T^{jet1}, (d) η^{jet1}, (e) E_T^{jet2} and (f) η^{jet2} after all cuts but the one on the plotted variable.*

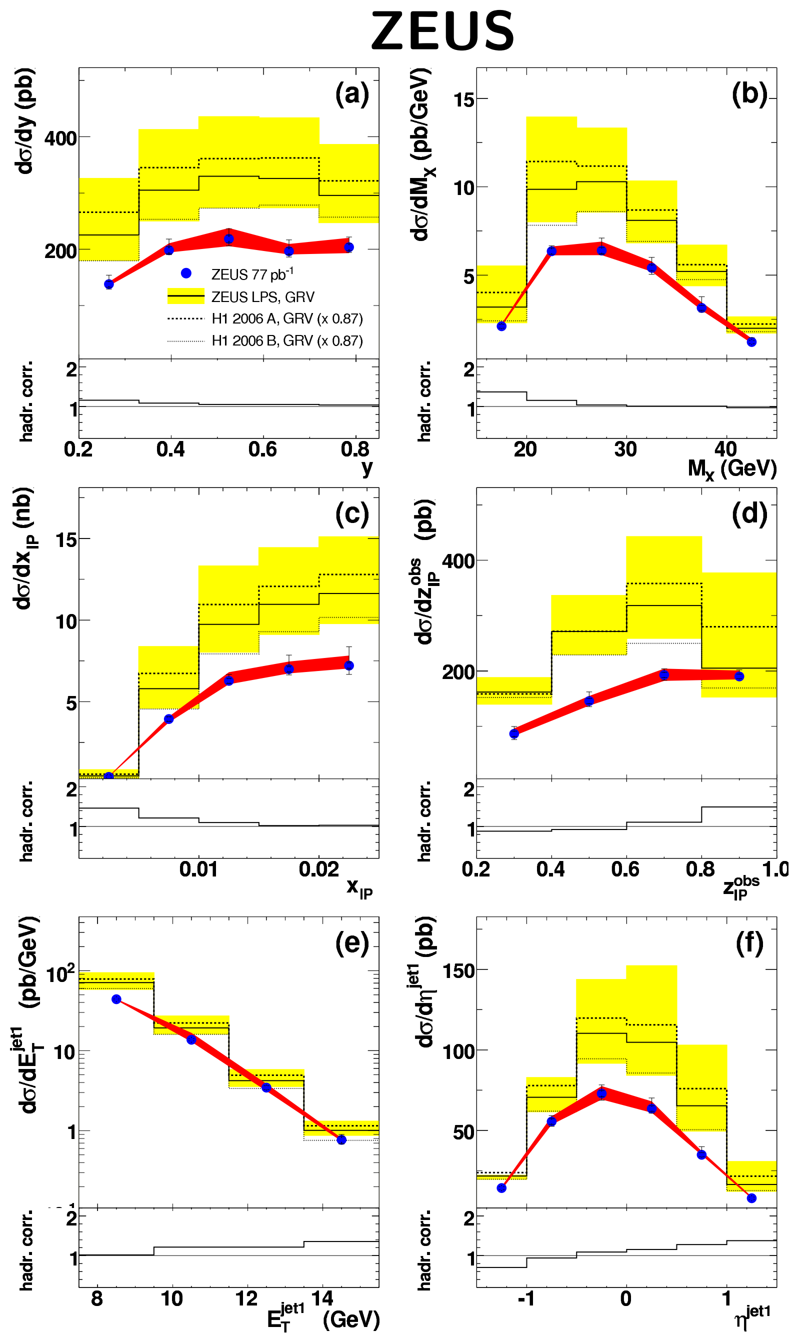

Figure 3: *Single-differential cross sections (dots) as a function of (a) y, (b) M_X, (c) x_{IP}, (d) $z_{IP}^{\rm obs}$, (e) $E_T^{\rm jet1}$ and (f) $\eta^{\rm jet1}$ compared with NLO QCD predictions, corrected for hadronisation, using the dPDFs from the ZEUS LPS fit (solid line), the H1 2006 fit A (dashed line) and the H1 2006 fit B (dotted line) and the GRV γ-PDFs. The inner error bars of the dots show the statistical uncertainty, the outer error bars show the statistical and systematic uncertainties (see Section 7) added in quadrature. The dark shaded band indicates the jet energy scale uncertainty. The light shaded band shows the theoretical uncertainty due to the variation of the scale when using the ZEUS LPS fit. Underneath each plot the hadronisation corrections applied to the NLO prediction at parton level are shown.*

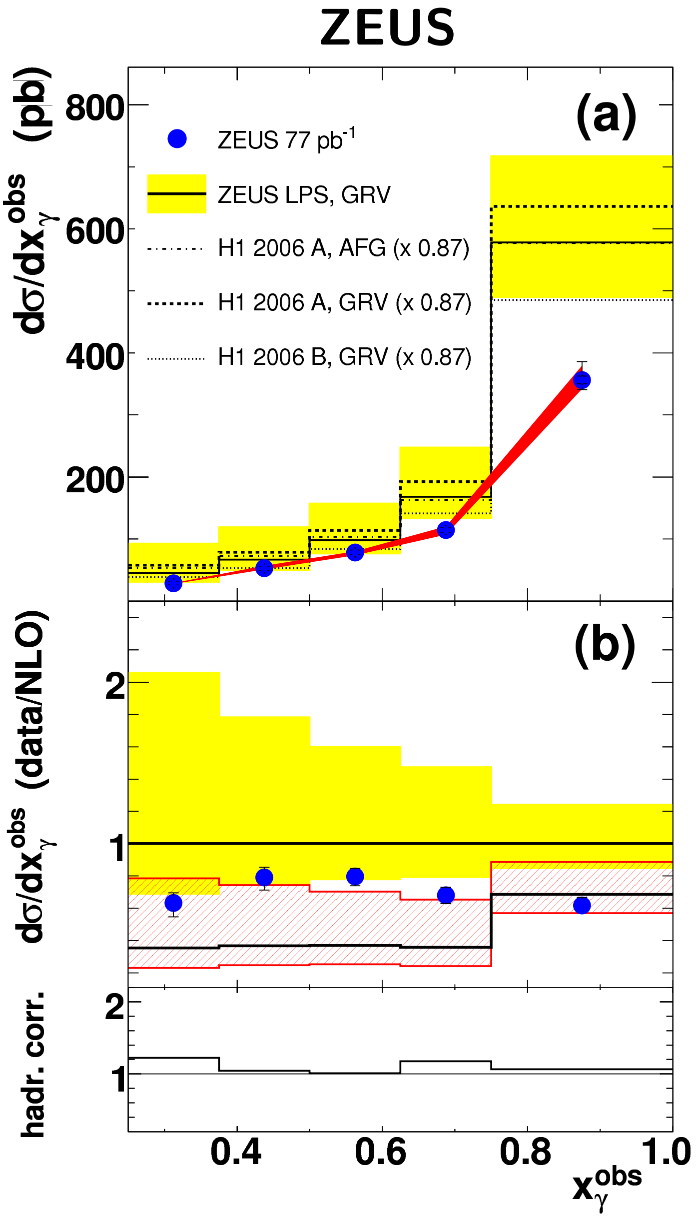

Figure 4: *(a) Single-differential cross section as a function of* $x_\gamma^{\rm obs}$ *compared with NLO QCD predictions, corrected for hadronisation, using the dPDFs from the ZEUS LPS fit (solid line), the H1 2006 fit A (dashed line) and the H1 2006 fit B (dotted line) and the GRV* γ*-dPDF. The prediction with H1 2006 fit A is also shown using the AFG parametrisation of the* $\gamma-$*PDFs (dashed-dotted line). Other details are the same as in the caption of Fig. 3. (b) Ratio of data and NLO predictions using the ZEUS LPS fit and GRV. The histogram indicates the expectation with the predicted resolved photon component scaled down by a factor of 0.34. The shaded and hatched bands show the theoretical uncertainty. Underneath the hadronisation corrections applied to the NLO prediction at parton level are shown.*

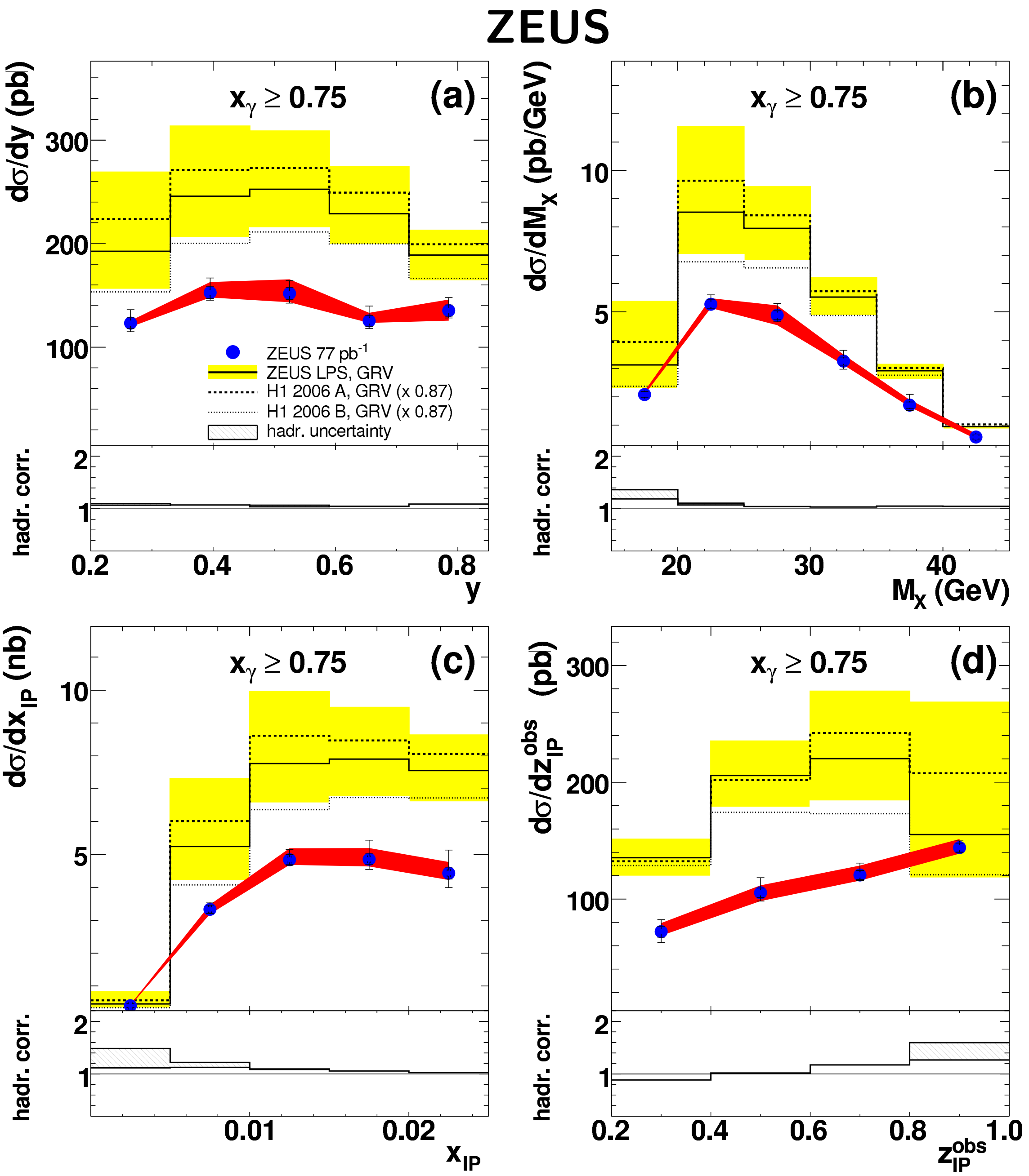

Figure 5: *Single-differential cross sections as a function of (a) y, (b) M_X, (c) x_{IP} and (d) $z_{IP}^{\rm obs}$ for direct-photon-enriched dijet photoproduction ($x_\gamma^{\rm obs} \geq 0.75$) compared with NLO QCD predictions, corrected for hadronisation, using the dPDFs from the ZEUS LPS fit (solid line), the H1 2006 fit A (dashed line) and the H1 fit B (dotted line) and the GRV γ-PDFs. Underneath each plot hadronisation corrections are shown which were obtained with* RAPGAP *(upper histogram) and* POMWIG *(lower histogram), respectively. The shaded bands indicate the differences. The corrections from* RAPGAP *were applied to obtain the NLO predictions shown above. Further details are the same as in the caption of Fig. 3.*

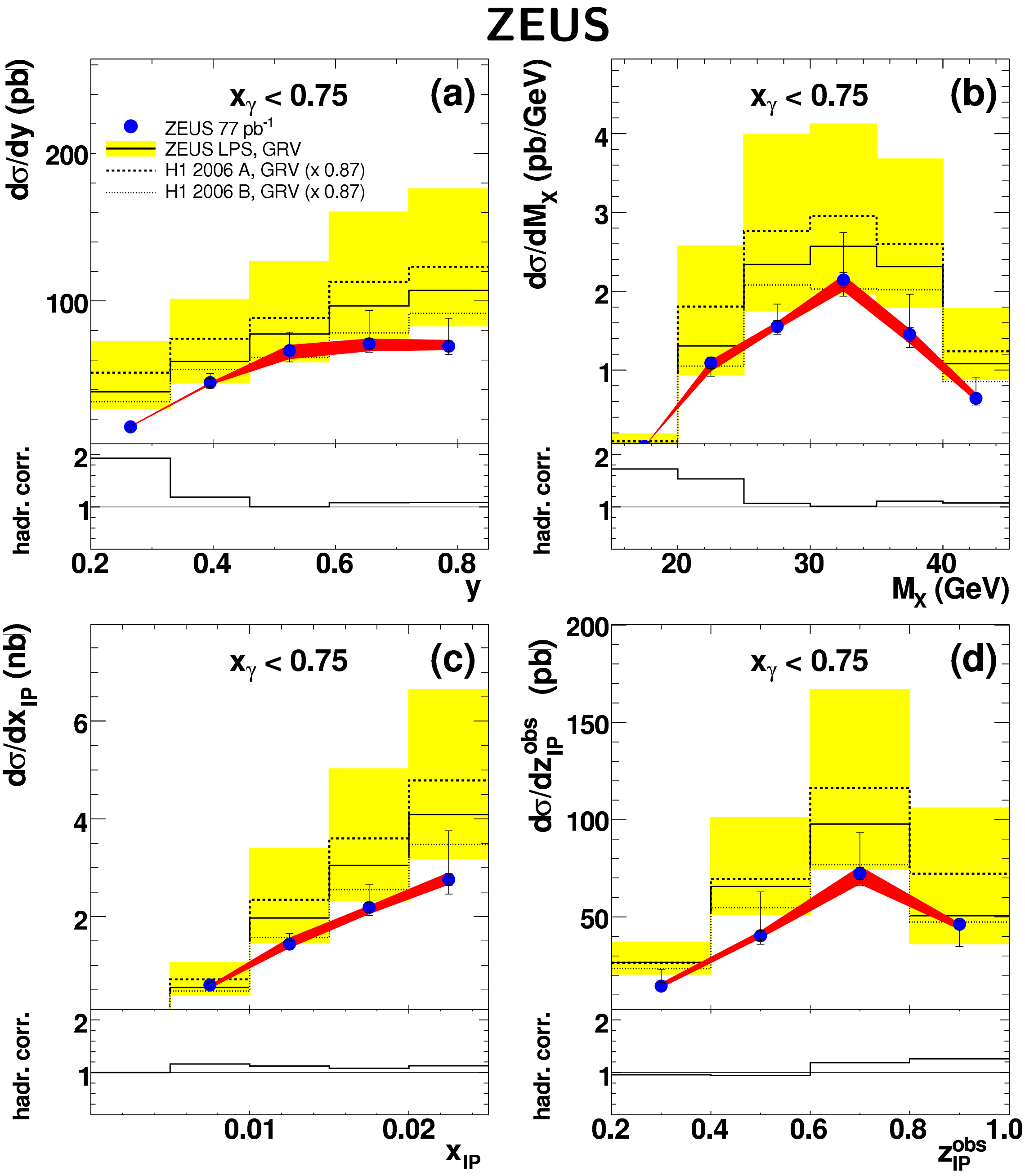

Figure 6: *Single-differential cross sections as a function of (a) y, (b) M_X, (c) x_{IP} and (d) $z_{IP}^{\rm obs}$ for resolved-photon-enriched dijet photoproduction ($x_\gamma^{\rm obs} < 0.75$) compared with NLO QCD predictions, corrected for hadronisation, using the dPDFs from the ZEUS LPS fit (solid line), the H1 2006 fit A (dashed line) and the H1 2006 fit B (dotted line) and the GRV γ-PDFs. Underneath each plot the hadronisation corrections applied to the NLO predictions at parton level are shown. Further details are the same as in the caption of Fig. 3.*